Academic Journal of Engineering and Technology Science
ISSN 2616-5767 Vol.3, Issue 8: 90-97, DOI: 10.25236/AJETS.2020.030810

Research on Large-Scale Solar Ray Tracing Based on Ray Adaptation

Zhi YAO[a], Junpeng Ren[b]

Faculty of Science, Xi'an Aeronautical University, Xi'an, Shaanxi 710000, China
[a]386645119@qq.com,[b]423458130@qq.com

ABSTRACT. *Accurate capture of solar rays can improve the solar energy utilization rate of solar devices, especially concentrated solar devices. The existing concentrated solar power generation system mainly adopts the methods of program control, sensor control and joint control of program and sensor. In order to improve the speed of ray tracing algorithm, a fast algorithm for traversing three-dimensional straight line uniform voxels is proposed. In this structure, the empty nodes of octree model are adaptively aggregated into bounding volumes, which reduces the intersection times of light and empty nodes as much as possible. Then, empty spatial grids are gathered adaptively with fewer empty boxes to speed up the calculation of ray tracing. The running speed of this algorithm is increased by about 56.5% compared with the existing fastest single-step algorithm, which greatly improves the efficiency of ray tracing, and can be realized only by using simple integer operation.*

KEYWORDS: *Ray tracing, Adaptive algorithm, Solar ray*

1. Introduction

As a clean and sustainable energy, solar energy is an ideal renewable energy. Although many acceleration structures such as KD-tree and hierarchical bounding box have been proposed, they are mainly used in static scenes but not in dynamic scenes because of the high cost of reconstructing them [1]. Ray tracing algorithm involves a large number of intersection calculations between rays and scenes. The efficiency of ray tracing algorithm is improved by improving the speed of intersection, reducing the number of intersection and increasing the interval of ray sampling, and adopting parallel algorithm [2]. The sensor control method is to measure the direction of sunlight in real time, but there is a tracking dead zone and a narrow tracking range in practical application; Ulseth [3] proposed a 3D DDA voxel traversal algorithm based on evenly dividing the space into voxels, which improved the efficiency of ray tracing. WANG [4] and others put forward several improved voxel traversal algorithms based on Müller algorithm. Some solar energy utilization has its own economy. With the development of science and technology and the technological breakthrough of human development and utilization of solar energy, the economy of solar energy utilization will become more obvious.

Based on the reference [9] and the adaptive algorithm, this paper proposes an

ISSN 2616-5767 Vol.3, Issue 8: 90-97, DOI: 10.25236/AJETS.2020.030810

efficient uniform voxel traversal algorithm for pure integer multi-step mixed mode. By adaptively clustering the empty nodes of octree into bounding volumes, the tracing rays can reach the intersecting patches faster, which reduces the computation of ray intersection in the blank area. Considering the influence of heat radiation and heat transfer in heat flow calculation, in order to calculate heat flow and stray light, the radiometric method commonly used in thermal simulation software has to be introduced.

2. Tracking Method

The purpose of ray (straight line) pixel traversal is to find out all pixels that a straight line passes through, and the process is similar to raster conversion of a straight line. The difference is that the straight line generation algorithm only needs to find out pixels whose distance from the straight line is not more than 1/2 pixel unit [6]. In addition, the coarse tracking accuracy must match the detection range of the sensor, and the sun spot must fall on the photocell of the sensor after the coarse tracking. Coding can speed up the process of node searching, improve ray tracing efficiency, and realize the mapping between logical layer and physical layer. Because the installation of the receiver is fixed, in order to reflect the solar radiation at all times of the day to the fixed receiver through the mirror, the mirror must be equipped with a tracking device, and the direction of the reflected light of the heliostat should remain unchanged during the tracking process.

When the angle between solar rays and photocell normal is θ, photocell outputs electromotive force: $U = K \cdot \phi$,In which ϕ is luminous flux-light energy passing through section S_1 , and K is proportional constant. $\phi = I \cdot S_1 = I \cdot S_0 \cdot \cos\theta$,Where I is illuminance-luminous flux per unit area. So, $U = K \cdot I \cdot S_0 \cdot \cos\theta$,Make $U_0 = K \cdot I \cdot S_0$, then

$$U = U_0 \cdot \cos\theta \left(-\pi / 2 \le \theta \le \pi / 2\right) \quad (1)$$

The curve relationship between the output voltage of photocell and the included angle θ can be obtained by formula (1), as shown in Figure 1

ISSN 2616-5767 Vol.3, Issue 8: 90-97, DOI: 10.25236/AJETS.2020.030810

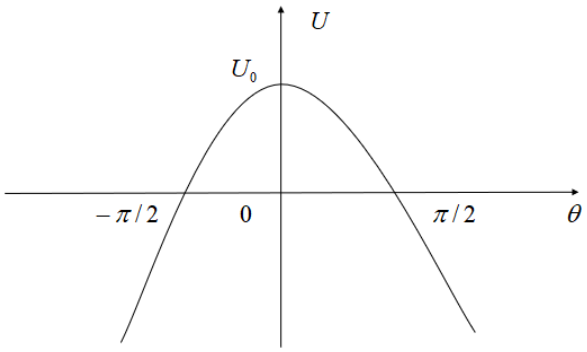

Fig.1 The Relationship between Output Voltage and of Photocell

In this paper, we present a new algorithm for calculating spatial grid resolution, which comprehensively considers patch distribution, number of spatial grid elements, number of spatial grid elements occupied by patches and creation time. The starting direction and position of each energy beam, the incidence and absorption or reflection of the energy beam on another surface, and the reflection direction of the energy beam are all related to a certain probability distribution function, that is, to pseudo-random numbers. By improving the tracking circuit, we can track the sunlight in the latitude direction. At the same time, all nodes no longer need to contain pointers to child nodes and parent nodes, and each leaf node only needs to store pointers to patches it contains (for real nodes and gray nodes) or pointers to the bounding volume of the node.

The four-quadrant photocell is placed in the center of the focal plane of the lens. At this time, the solar rays pass through the lens and get a solar image on the focal plane of the lens. In theory, the sundries on the lens surface have no effect on the intensity distribution of the solar image on the focal plane, which can improve the tracking stability of the sensor. In this paper, we only discuss the case of traversing straight line pixels in the first 1/8 quadrant (straight line slope k satisfies $0 \leqslant k1$), and straight lines in other quadrants can be obtained by symmetry. The control system determines the immediate sun position according to the geographical and time parameters provided, so as to ensure the accurate positioning of the system and the high accuracy and reliability of tracking.

3. Implementation of Control System

3.1 Sensor Detection Range

In order to describe the relationship between the logical position and the actual

ISSN 2616-5767 Vol.3, Issue 8: 90-97, DOI: 10.25236/AJETS.2020.030810

position of each node, the coding of nodes can be expressed in the form of general grid coordinates (x,y,z) . In order to eliminate the influence of program implementation on the experiment as far as possible, the algorithm overhead is measured by four parameters unrelated to computer hardware configuration, except the time of creating spatial grid. If ray tracing method is used alone, it is slightly insufficient for multiple diffuse reflection, and if radiance method is used alone, it is also inappropriate for specular reflection. Therefore, it is necessary to combine the two methods and complement each other. For the 180° jump after overnight, a travel switch can be added to the circuit, so that the circuit can automatically drive the system to reverse to sunrise angle after sunset, and the jump caused by rainy days can be solved by the positioning plate.

Let D be the diameter of photocell, f be the focal length of lens, θ be the angle between the incident ray of sun and the main optical axis, and d be the diameter of the solar image on photocell. Direct radiation from the sun is incident on the earth's surface with a sun angle of 32' [7]. According to the principle of geometrical optics, it can be concluded that θ should be small enough to make the spot of the sun image fall on the photocell. If the light spot falls on the photoelectricity, there is the following relationship:

$$\theta \le arc\tan(D/2f) - 16' \quad (2)$$

$$d \approx f \cdot \tan(32') \quad (3)$$

It can be known from formula (2) and formula (3) that when the diameter of the photocell is constant and the light spot completely falls on the photocell, the larger the focal length f is, the larger the d is and the smaller the θ is. That is, the longer the focal length is, the bigger the solar image is, and the smaller the range of solar rays that photocell can detect.

It can be known from formula (2) and formula (3) that when the diameter of the photocell is constant and the light spot completely falls on the photocell, the larger the focal length f is, the larger the d is and the smaller the θ is. That is, the longer the focal length is, the bigger the solar image is, and the smaller the range of solar rays that photocell can detect.

The total number of spatial grid elements, the total number of pointers contained in the spatial grid, the average number of spatial grid elements traversed by each ray and the average number of intersections between each ray and triangular patches. The bounding volume is constantly updated in the octree merging process, and all the nodes participating in the bounding volume merging point to the bounding volume, so there is no need to store it repeatedly. Serial communication module, event manager, A/D converter and other modules are integrated inside, which can meet the functional requirements of the control system. At the same time, it can realize simple floating-point operation and meet the requirements of coarse tracking

ISSN 2616-5767 Vol.3, Issue 8: 90-97, DOI: 10.25236/AJETS.2020.030810

calculation. In the whole control system diagram, the analog and switch values are collected by the peripheral circuit and input to the control port of the single chip microcomputer, processed by the single chip microcomputer and then output to the control part, and the corresponding actions are executed to complete the control of the whole system.

3.2 Intersection Test of Tracing Ray and Merging Node

In the ray intersection test, the ray and merged bounding volume can cross several blank nodes at one time, without intersecting with the boundary of each node, thus reducing the times of ray intersection test in empty area and improving the speed of tracking algorithm. Each empty cell has a pointer to the empty box that covers it. Because we use empty boxes to speed up the travel of light in the blank area, the smaller the number, the better. To a certain area in the illumination map, no two triangular patches will share the same area. In order to avoid the influence of grid division on the radiance algorithm, the idea of photon mapping is introduced to make the radiance correspond to the value of the illumination map.

In order to simplify the calculation, the algorithm assumes that the radiance is constant over the whole patch, which means that to accurately calculate the scene, it is necessary to divide the scene into fine geometric partitions, and the light energy transmission amount can be calculated by using the known reflectivity of the reflecting surface and the shape factor between two patches [8]:

$$B_i = E_i + R_i \sum_{j=1}^{n} B_j F_{ji} \tag{4}$$

Where B_i and B_j are the radiance of patches i and j respectively, R_i is the reflection coefficient of patch i, E_i is the energy emitted by patch i, and F_{ji} is the shape factor between patch i and patch j.

When the light deviates from the tracking range for some reason, the light will irradiate one of the two positioning plates (the light will not irradiate the positioning plate during normal operation), and the temperature of the irradiated positioning plate will definitely increase. When a 3D object is projected into a 2D space based on parameterization of the normal principal axis, the component corresponding to the normal principal axis is discarded and the other two components are retained. We adopt a simple creation method. Although it can't guarantee to produce the least empty boxes, it can produce enough empty boxes to draw dynamic scenes efficiently. Therefore, when designing, we should consider increasing the focal length of the lens to improve the resolution of the sensor, and also consider that the tracking accuracy of the selected coarse tracking algorithm should be consistent with the detection range of the sensor, so as to ensure that the sun spot can fall on the photocell after coarse tracking.

ISSN 2616-5767 Vol.3, Issue 8: 90-97, DOI: 10.25236/AJETS.2020.030810

It is now stipulated that the balance position of the switch contact is the working point when the light spot does not illuminate any temperature sensitive switch. Assuming that the annual variation range of ambient temperature is ΔT_y (its order of magnitude is 10) and l is the moving range of the switch equilibrium position, there is [9]:

$$\frac{\Delta T}{\Delta h} = \frac{\Delta T_y}{l} \quad (5)$$

If the temperature difference between winter and summer is large and the moving range of the working point is large, some measures can be taken to control the position of the working point.

The speed of traversal algorithm is mainly determined by the iterative calculation of δ_{xy} and δ_{xz}, the logical operation to control the traversal process and the number of multiplications of τ_{xy} and τ_{xz}. They are coarse positioning photocell voltage sum signal, azimuth direction voltage difference signal, height angle direction voltage difference signal, fine positioning photocell voltage sum signal, azimuth direction quadrant voltage difference signal and height angle direction voltage difference signal. The system mainly completes the functions of coarse tracking sun position calculation, tracking signal detection, motor driving, position detection, display, monitoring and so on. Tracking solar rays can be divided into coarse tracking and fine positioning. The tracking circuit returns to normal working state. This process may take a long time, from several minutes to ten minutes, which is called positioning time.

4. Result Analysis

The experiment was carried out on a PC equipped with a 3.0GHz dual-core Xeon CPU, 3 .0GB memory and Windows XP operating system. Because different local environments are very different, only the method of parameter setting is given, but no specific optimal value is given. All parameters are interrelated, so when setting parameters, we should consider all parameters comprehensively instead of one parameter alone. All kinds of tracking information of the system can be transmitted to the upper computer through RS485 bus, and the upper computer can also control the tracking device, including starting tracking, returning to zero, stopping and other commands. The simulation calculation of illumination simulation is carried out, and the model. prt file is processed in a series, which is converted into an. x file containing spatial coordinates, texture coordinates and material properties, and then imported into the program for calculation.

Table 1 shows the average number of additions and multiplications consumed by the algorithm in this paper and the algorithm in reference [9] in traversing each voxel in three cases. It can be seen from table 1 that compared with the algorithm in

ISSN 2616-5767 Vol.3, Issue 8: 90-97, DOI: 10.25236/AJETS.2020.030810

reference [9], for the first and third cases, the number of addition operations consumed in this paper is reduced by about 34.0% and 13% respectively, and the number of multiplication operations is basically the same; For the second case, the operation times of addition and multiplication in this paper are reduced by about 18% and 32.6%, respectively.

Table 1 Comparison between The Algorithm in This Paper and the Algorithm in Literature [9] in the Amount of Computation Per Step

Algorithm	Situation (1)		Situation (2)		Situation (3)	
	Addition	Multiplication	Addition	Multiplication	Addition	Multiplication
This algorithm	1.22	0.027	2.20	0.17	3.08	0.25
The algorithm in reference [9]	5.27	0.048	4.22	0.55	3.85	0.27

Table 2 Various Traversal Algorithms Take Up Cpu Time

Algorithm	This algorithm	Literature [9]	Zemcik	Müller
Execution time	0.011	0.028	0.013	0.104

In order to compare the overall efficiency of the algorithms, the four algorithms in Table 2 are implemented in C++ language on Lenovo notebook computer with CPU frequency of 2.33GHz. A total of 2103 straight line samples in Table 1 are actually drawn, and the average CPU execution time of each algorithm (excluding voxel output operation) is calculated. Compared with the algorithm in [9], the average efficiency of this algorithm is improved by 56.5%, nearly 17 times and 12 times higher than Zemcik algorithm and Müller algorithm, respectively.

5. Conclusions

When dealing with large-scale dynamic scenes, it is very important not only to use acceleration structure to greatly improve the traveling speed of light, but also to quickly reconstruct acceleration structure. Aiming at the problem of solar illumination simulation analysis of space remote sensors, this paper comprehensively considers various simulation analysis methods, and puts forward a new analysis idea, that is, illumination diagram method which combines global illumination radiance method and ray tracing method. The temperature sensitive switch works by the temperature difference between the two temperature sensitive switches caused by the thermal effect of sunlight, so the system will not work on cloudy days or at night with moonlight, and the whole system will start to work only

ISSN 2616-5767 Vol.3, Issue 8: 90-97, DOI: 10.25236/AJETS.2020.030810

when the light intensity reaches the set threshold, which can not only avoid misoperation, but also reduce the running power consumption of the whole system. With the development of programmable GPU technology, researchers pay more and more attention to the application of parallel computing in ray tracing. Therefore, the next step should consider further improving the ray tracing algorithm and its acceleration structure by parallel processing, so as to achieve the optimal configuration on GPU.

References

[1] Hee M S, Seok L J, Hwan S I. Ray-Tracing-Based Modeling of Clad-Removed Step-Index Plastic Optical Fiber in Smart Textiles: Effect of Curvature in Plain Weave Fabric. Advances in Materials Science and Engineering,2018,(2018-3-29), 2018, 2018:1-16.

[2] Huang Minghui. Study on the performance of box solar furnace by ray tracing. Journal of the United Nations General Assembly, vol. 14, no. 1, pp. 129-145, 2017.

[3] Ulseth J, Zhu Z, Sun Y, et al. Accelerated X-Ray Diffraction (Tensor) Tomography Simulation Using OptiX GPU Ray-Tracing Engine. IEEE Transactions on Nuclear Science,no. 99, pp. 1-1, 2019.

[4] WANG, Rui, SUN, et al. Analysis and evaluation of band-limited ray tracing method. Global Geology, vol. 21, no. 03, pp. 55-60, 2018.

[5] Shang C, Teng P, Lyu J, et al. Infrasonic source altitude localization based on an infrasound ray tracing propagation model. The Journal of the Acoustical Society of America, vol. 145, no. 6, pp. 3805-3816, 2019.

[6] Ren Wei. the design of solar ray tracking circuit. industrial technology and vocational education, vol. 015, no. 004, pp. 5-7, 2017.

[7] Zhang Man. Research on ray tracing acceleration technology based on KD-tree. Computer Products and Circulation, no. 09, pp. 121-121, 2019.

[8] Li Shaohua, Wang Liwei, Liao Mingjun. Influence of dish solar collector structure on thermal radiation. Journal of North China Electric Power University no. Natural Science Edition), vol. 45, no. 05, pp. 89-93, 2018.

[9] Shi Zheng-Jin, Guo Rui-Xi, Huang Fu Shang-wei, et al. Research on maximum power tracking method of solar power generation. Science and Technology Information, vol. 016, no. 026, pp. 15-18, 2018.